

Numerical Modeling of Argon-Oxygen Decarburization Slag Cooling

Aki Kärnä, Ville-Valtteri Visuri,* Eetu-Pekka Heikkinen, Petri Sulasalmi, Pauli Torvinen, Juha Koskinen, and Timo Fabritius

Stainless steelmaking produces different types of slags which need to be cooled, stored, and pretreated before further use. In current practice, the slag is cooled in an air atmosphere, but water cooling has been envisaged to speed up cooling. The aim of this article is to simulate the cooling of argon-oxygen decarburization (AOD) slag under the conditions of ambient cooling and water cooling. The effects of the thickness and initial temperature of the slag layer are also studied. Finally, practical means to improve the cooling practice are evaluated based on the model predictions.

1. Introduction

Global stainless steel production was 50.7 million tons in 2018,^[1] whereas the most common process for refining stainless steel is argon-oxygen decarburization (AOD).^[2] Depending on the steel grade, the amount of AOD slag produced is roughly 100–200 kg ton⁻¹ of steel.^[3] A significant amount of research effort has been directed toward studying various aspects of slag practice in the AOD process. Topics studied include the evolution of slag composition^[4–7] and physical properties^[8] during processing as well as the effect of slag on refractory wear,^[9–11] fluid flows,^[12,13] bath mixing,^[12,13] and vessel oscillation.^[14]

The produced AOD slag needs to be cooled before further utilization. During slow cooling, the AOD slag undergoes a phase transformation of β -dicalcium silicate to γ -dicalcium silicate at approximately 773–723 K (500–450 °C), resulting in disintegration of the slag due to the associated 10–12% volume

expansion.^[15] Consequently, different chemical stabilization techniques have been proposed.^[16] Borate additions are a well-known stabilization method,^[16,17] whereas nonboron additions such as MgO, Al₂O₃, Fe₂O₃, BaO, K₂O, P₂O₅, and Cr₂O₃ have been reported to stabilize stainless steel slags.^[16] Furthermore, the properties of the slag are affected by the cooling method.^[18–21] The simplest method for AOD slag cooling is cooling in an ambient atmosphere in a slag yard,^[15] but other methods, such as water cooling^[22] or air-

granulation,^[15] have been proposed for achieving a faster cooling rate. The literature on modeling the cooling of AOD slags remains scarce. Kriskova et al.^[18] proposed a 1D model for calculating the cooling rate of granulated AOD slag in a cooling drum. Pandelaers et al.^[23] studied the ambient cooling of a multilayer slag bed with a numerical model and experiments. Although the heat transfer associated with spray cooling has been studied extensively,^[24–27] there have not been any attempts to model the evolution of the slag temperature during water cooling. The aim of this article is to first study the cooling of slag in an ambient atmosphere, and then to extend this approach for the water cooling of slag.

2. Description of the Model

A single layer of slag is considered with a 1D model. This simplification is justified by the fact that the width and length of the slag layer are much larger than the height of the layer.^[23,28] The calculation domain consists of a base layer representing the ground and a slag layer on top (see **Figure 1**). Both layers are divided into 50 control volumes with equal height and additional computational nodes set at the material boundaries.


The conservation equations are constructed according to the finite volume method. The time integration of the equations is conducted using the implicit Euler method, which is stable with variable material properties, such as the heat capacity of the slag. The discretized equation for slag top surface calculation node in the case of air cooling is

$$\frac{k_s(T_1 - T_{\text{surf}})}{0.5 \Delta x} = \alpha_a(T_{\text{amb}} - T_{\text{surf}}) + \sigma_r \epsilon (T_{\text{amb}}^4 - T_{\text{surf}}^4) \quad (1)$$

where k_s is the heat conductivity of slag, T_1 is the temperature of the top cell, T_{surf} is the surface temperature of the slag, Δx is the cell spacing, α_a is the heat transfer coefficient, T_{amb} is the

Dr. A. Kärnä, Dr. V.-V. Visuri, Dr. E.-P. Heikkinen, Dr. P. Sulasalmi, Prof. T. Fabritius
Process Metallurgy Research Unit
University of Oulu
PO Box 4300, 90014 Oulu, Finland
E-mail: ville-valtteri.visuri@oulu.fi

P. Torvinen, J. Koskinen
Tapojärvi Oy
Tullipuistonkatu 2, 95400 Tornio, Finland

 The ORCID identification number(s) for the author(s) of this article can be found under <https://doi.org/10.1002/srin.202000054>.

© 2020 The Authors. Published by WILEY-VCH Verlag GmbH & Co. KGaA, Weinheim. This is an open access article under the terms of the Creative Commons Attribution-NonCommercial-NoDerivs License, which permits use and distribution in any medium, provided the original work is properly cited, the use is non-commercial and no modifications or adaptations are made.

DOI: 10.1002/srin.202000054

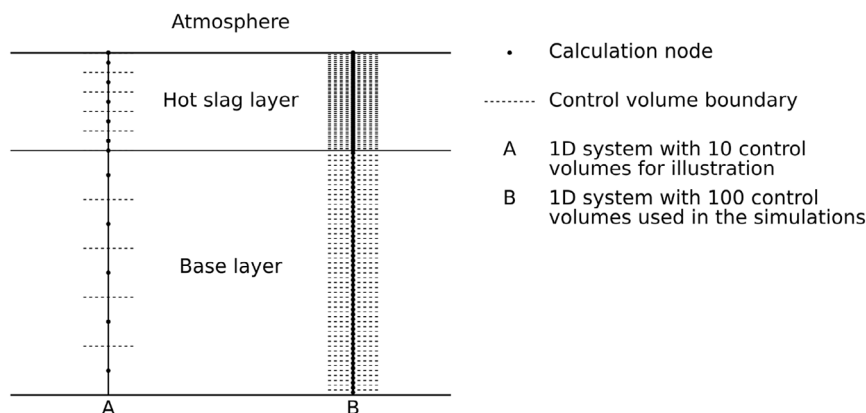


Figure 1. A schematic illustration of the calculation domain.

ambient temperature, ε is the emissivity, and σ_r is the Stefan-Boltzmann constant. The first cell next to slag top surface is represented by

$$\frac{k_s(T_{\text{surf}} - T_1)}{0.5 \Delta x} + \frac{k_s(T_2 - T_1)}{\Delta x} = \rho_s \Delta x c_{p,s}(T_1 - T_{1,\text{old}}) \quad (2)$$

where T_2 is the temperature of the cell next to slag top surface, ρ_s is the density of the slag, $c_{p,s}$ is the specific heat capacity of slag, and $T_{1,\text{old}}$ is the temperature T_1 of the previous time step. The cells inside the slag layer, the cell next to slag-ground boundary, and the node at the boundary are represented by Equation (3), (4), and (5), respectively.

$$\frac{k_s(T_{i-1} - T_i)}{\Delta x} + \frac{k_s(T_{i+1} - T_i)}{\Delta x} = \rho_s \Delta x c_{p,s}(T_i - T_{i,\text{old}}) \quad (3)$$

$$\frac{k_s(T_{i-1} - T_i)}{\Delta x} + \frac{k_s(T_b - T_i)}{0.5 \Delta x} = \rho_s \Delta x c_{p,s}(T_i - T_{i,\text{old}}) \quad (4)$$

$$\frac{k_s(T_{i-1} - T_b)}{0.5 \Delta x} = \frac{k_{\text{ground}}(T_b - T_{0,\text{ground}})}{0.5 \Delta x} \quad (5)$$

where T_{i-1} is the temperature of the previous cell ($i - 1$), T_{i+1} is the temperature of the next cell ($i + 1$), T_b is the temperature of the boundary, k_{ground} is the heat conductivity of the ground, and $T_{0,\text{ground}}$ is the initial temperature of the ground. The nodes and cells at the ground layer are formulated similar to Equation (5) with ground properties instead of slag properties. In the cases studied in this article, the ground material is slag and the properties are assumed to be equal. From the conservation equations and derivatives in respect to all temperature variables, a tridiagonal matrix is formed, and the solution is obtained by the Thomas algorithm. The convergence was assessed in terms of l_2 norm, for which a criterion of $l_2 = 10^{-8}$ was used.

2.1. Material Properties and Boundary Conditions

Phase transitions in the slag are taken into account in the model via heat capacity. The specific heat capacity c_p is extracted from slag enthalpy calculations, which were executed with FactSage version 7.2 and its FTToxid and FactPS databases. Enthalpy

Table 1. Slag composition considered in the enthalpy calculations.

Composition [wt%]							
CaO	SiO ₂	MgO	Fe ₂ O ₃	Cr ₂ O ₃	Al ₂ O ₃	TiO ₂	CaF ₂
53.6	26.6	7.7	1.0	1.0	1.9	0.5	7.7

changes for an oxide system with a composition presented in **Table 1** were computed by assuming that the system consists of the most stable phases at a given temperature, and consequently relevant phase transformations are automatically accounted for. **Figure 2** shows the calculated enthalpy change and liquid fraction of the slag as a function of temperature. The results indicate that the slag remains partly liquid until 1090 °C.

The physical properties used are shown in **Table 2**. The thermal conductivity of slag varies not only as a function of its temperature and composition but also as a function of the porosity of the slag. The value of the thermal conductivity is expected to vary between 0.5 and 2.5 W m⁻¹ K⁻¹.^[29] A value of 1.25 W m⁻¹ K⁻¹ was found to give best results in the study of Pandelaers et al.^[23] for electric arc furnace and AOD slags. The effect of

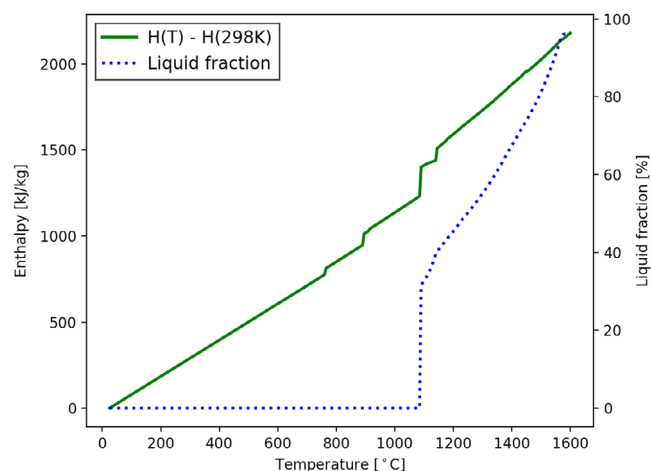


Figure 2. Enthalpy change and liquid fraction of the slag as a function of temperature.

Table 2. Physical properties employed.

	Unit	Slag	Air	Ground
Density	kg m ⁻³	2700 ^[29]	–	Same as that of slag
Emissivity	–	0.9	–	–
Initial temperature	K (°C)	1873.15 (1600)	293.15 (20)	293.15 (20)
Thermal conductivity	W m ⁻¹ K ⁻¹	1.25	–	Same as that of slag
Ambient cooling				
Convective heat transfer coefficient	W m ⁻² K ⁻¹		20	
Water cooling				
Droplet diameter of water spray	m		0.001	
Initial temperature of water	K (°C)		293.15 (20)	
Latent heat of vaporization of water	J kg ⁻¹		2 257 000 ^[36]	
Boiling point of water	K (°C)		373.15 (100) ^[36]	
Surface tension of water ^{a)}	N m ⁻¹		0.07286 ^[37]	
Specific heat capacity of water vapor ^{b)}	J kg ⁻¹ K ⁻¹		2080 ^[38]	
Specific heat capacity of liquid water ^{a)}	J kg ⁻¹ K ⁻¹		4182 ^[38]	
Density of water ^{a)}	kg m ⁻³		998.21 ^[38]	

^{a)}At 293.15 K (20 °C) and 1 atm; ^{b)}At 373.15 K (100 °C) and 1 atm.

different values was studied and is illustrated later. For the sake of simplicity, a constant value of slag density was used in the calculations. The slag density was estimated to be 2700 kg m⁻³,^[29] which is close to the value of 2650 kg m⁻³ used by Pandelaers et al.^[23] The ground below the slag layer consists of cooled slag, with the same physical properties. The initial temperature of the slag layer is set at 1873.15 K (1600 °C) and the ground at 293.15 K (20 °C). A constant temperature of 293.15 K (20 °C) is used at the lower boundary of the ground layer. At the slag top, a heat transfer coefficient of 20 W m⁻² K⁻¹ was used for air cooling together with an emissivity of 0.9 for radiation heat transfer. As an initial approximation, the water droplet size was assumed to be 1 mm. As it will be shown later, the surface of the slag cools very rapidly and consequently, the water droplet diameter has virtually no effect on the predicted cooling rate of the slag.

The heat transfer coefficient at the upper surface can be defined as

$$\alpha = \frac{q''}{T_{\text{amb}} - T_0} \quad (6)$$

where q'' is the heat flux. In the case of water cooling, two models for water sprays are used: a model from Yao and Cox^[30] for small water fluxes, and a model from Wendelstorf et al.^[31] for larger fluxes. In the model of Wendelstorf et al.,^[31] the cooling effect of water spray is described with a heat transfer coefficient as

$$\alpha = 190 + \tanh\left(\frac{G}{8}\right) \left(140G \left(\frac{1 - G\Delta T}{72000} \right) + \left\{ 3.26\Delta T^2 1 - \tanh\left(\frac{\Delta T}{128}\right) \right\} \right) \quad (7)$$

where G is the water spraying rate and $\Delta T = T_{\text{surf}} - T_1$ is the temperature difference between the surface and the water. Equation (7) is valid for $T_{\text{surf}} = 200\text{--}1100$ °C and

$G = 3\text{--}30$ kg m⁻² s⁻¹.^[31] This model has been successfully applied in numerical models for quenching applications.^[32,33] In the model of Yao and Cox,^[30] the heat transfer efficiency for water spray was expressed as the ratio of the heat transfer rate to the theoretically maximal heat transfer rate

$$q'' = \epsilon \left[G(\Delta h_{\text{lg}} + c_{p,l}(T_{\text{sat}} - T_1) + c_{p,v}(T_0 - T_{\text{sat}})) \right] \quad (8)$$

$$\epsilon = 8 \times 10^{-7} \left(\frac{\text{We}_s T_{\text{sat}}}{\Delta T} \right)^{-0.62} + 3.5 \times 10^{-3} \left(\frac{\text{We}_s T_{\text{sat}}}{\Delta T} \right)^{-0.2} \quad (9)$$

where Δh_{lg} is the latent heat of vaporization, $c_{p,l}$ is the specific heat capacity of water, T_{sat} is the saturation temperature of water (boiling point), $c_{p,v}$ is the specific heat capacity of water vapor, and We_s is the modified Weber number, which is defined as follows

$$\text{We}_s = \frac{G^2 d}{\rho_l \sigma_1} \quad (10)$$

where d is the water droplet diameter and σ_1 is the surface tension of water. The model of Yao and Cox^[30] (Equation (9)) is valid for $T_{\text{surf}} = 300\text{--}800$ °C and $G = 0\text{--}50.5$ kg m⁻² s⁻¹. **Figure 3** shows the predicted heat flux as a function of water flux with two slag surface temperatures: 500 and 100 °C. It can be seen that the model of Yao and Cox^[30] tends to predict much lower heat fluxes than the model of Wendelstorf et al.^[31]

3. Results and Discussion

3.1. Model Verification

The model was tested with a simple case of a flat plate with constant temperatures at both sides. The material properties were chosen to correspond to the AOD slag, but with constant values.

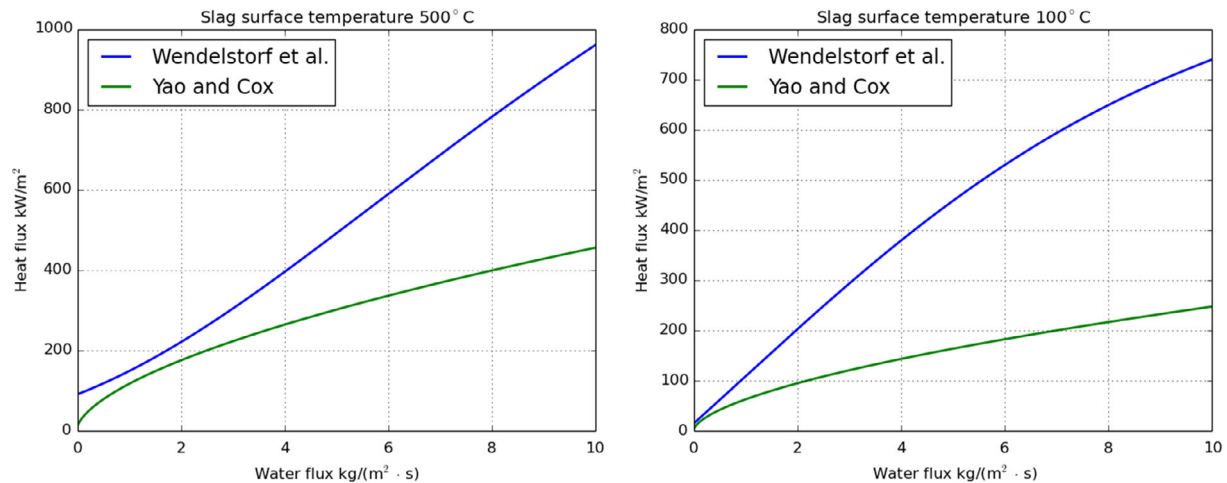


Figure 3. Heat flux as a function of water flux calculated using the correlations of Wendelstorf et al.^[31] and Yao and Cox^[30] with two slag surface temperatures: 500 °C (left) and 100 °C (right).

The initial temperature was set to 1600 °C and the boundary temperatures to 20 °C. With the help of simplifications, a corresponding case is possible to solve analytically for comparison. The analytical result is given by the Fourier series solution. The result from the implicit numerical model was compared with the analytical solution in **Figure 4, 5, 6**. Figure 4 shows the slag layer center temperature as a function of time. Figure 5 shows the temperature profiles across the slag layer at different times, whereas Figure 6 shows the temperature profiles as a function of time. The simulated result and the analytical solution agree very well in all three figures.

3.2. Cooling with Ambient Air

In the case of cooling the slag in the yard without water, heat is transferred to the atmosphere with convection heat transfer and radiation heat transfer, of which radiation is much more effective at high temperatures. The convective heat transfer coefficient

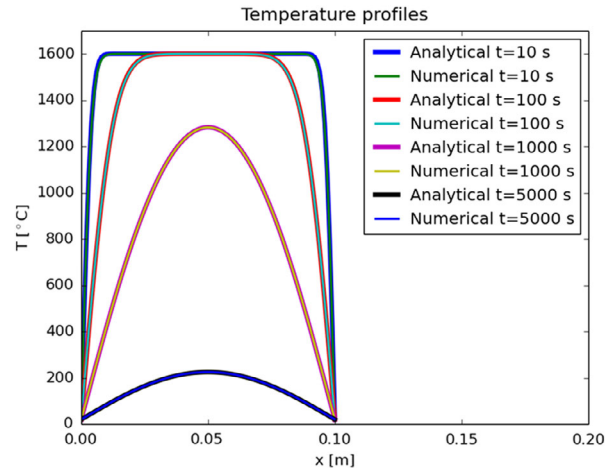


Figure 5. Temperature profiles at different times in a test case (ambient air cooling, slag layer height = 0.1 m).

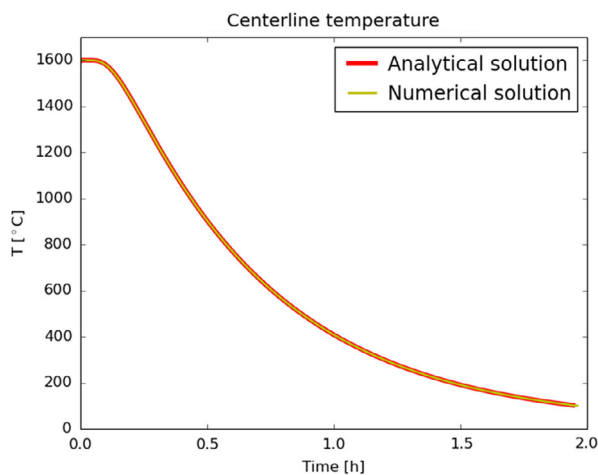


Figure 4. Centerline temperature as a function of time in a test case (ambient air cooling, slag layer height = 0.1 m).

was estimated to be $20 \text{ W m}^{-2} \text{ K}^{-1}$. Conductive heat transfer cools the slag from below.

A single simulation with a slag layer of 0.2 m and a thermal conductivity of $1.25 \text{ W m}^{-1} \text{ K}^{-1}$ is shown in **Figure 7, 8**. Figure 7 shows that the surface of the slag layer cools much faster than the center of the slag layer. Comparison with Figure 2 suggests that the center part of the slag becomes solid only after 4.6 h. As shown in Figure 8, the hottest part of the slag is slightly below the center of the slag layer (-0.1 m), which indicates that heat transfer to ambient air is more efficient than heat transfer to the ground below the slag.

To illustrate the effect of different values of thermal conductivity to the cooling times of slag, several cases are calculated until the average temperature in the slag is 100 °C. As all the cells in the slag phase have equal thicknesses, the average temperature corresponds to the arithmetic mean of the cell temperatures. The time required to reach the average temperature is shown in **Figure 9**.

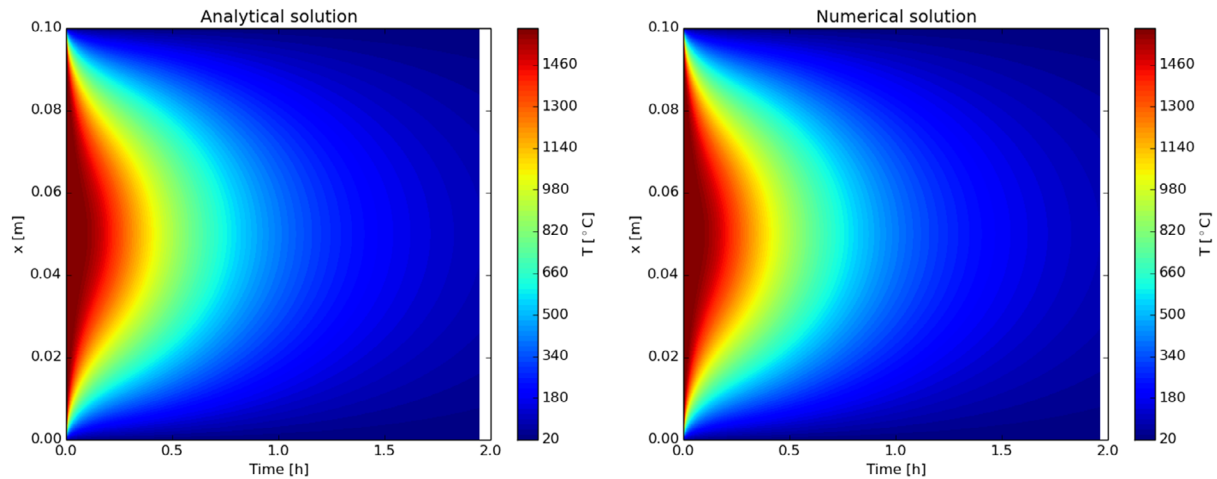


Figure 6. Temperature profile as a function of time in a test case (ambient air cooling, slag layer height = 0.1 m).

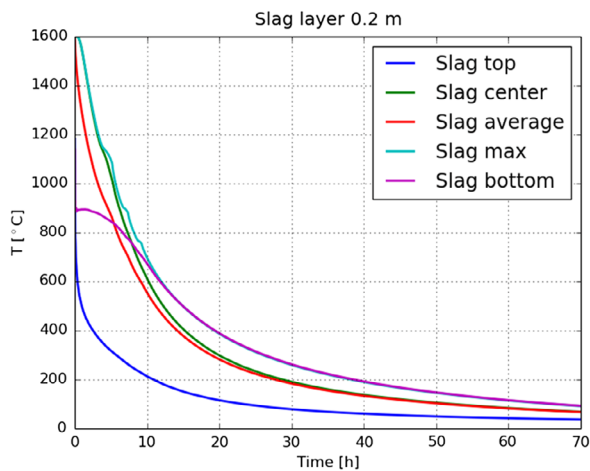


Figure 7. Time evolution of slag temperature with $k = 1.25 \text{ W m}^{-1} \text{ K}^{-1}$.

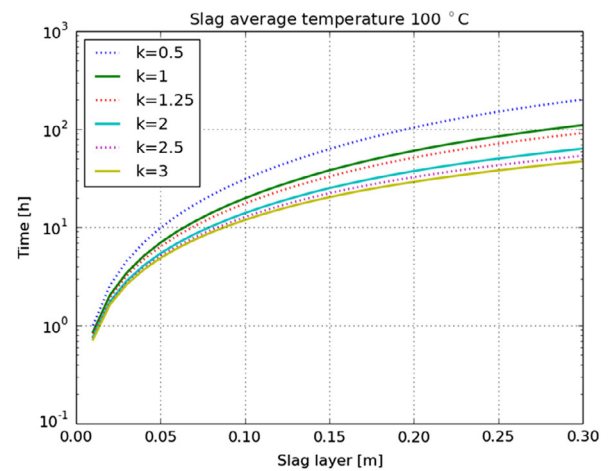


Figure 9. Cooling time from 1600 to 100 °C as a function of slag layer thickness with different heat conductivities of slag.

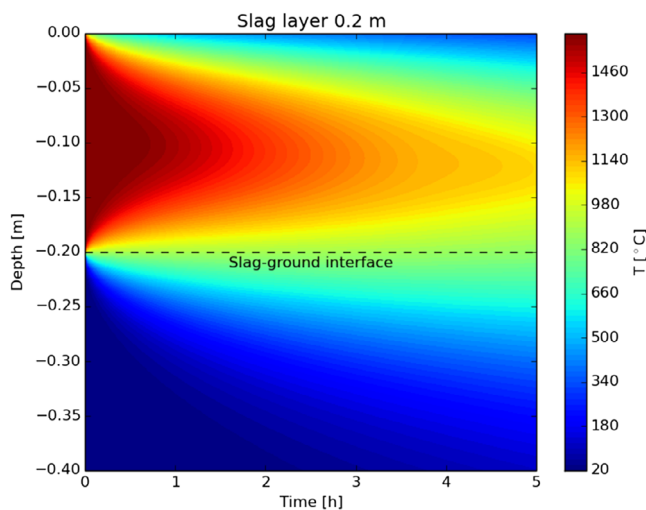


Figure 8. Ambient cooling temperature profiles as a function of time.

3.3. Water Cooling

The cases of water cooling were simulated in the same manner as air cooled cases, with an additional variable of the water spraying rate (see **Figure 10**). Although water cooling cools the slag surface efficiently with all the studied water feeding rates, there is not much difference in the cooling times. However, in comparison with air cooling, there is a clear difference. The slag thermal conductivity is low and little water is required to cool the surface. In any case, the cold surface has a limited effect on the cooling speed. In practice, the water-cooled simulations give the maximum cooling rate for cooling a slag layer from the top surface. For faster cooling, the slag layer should be broken to increase the interfacial area between slag and water.

As for the utilization of solidified slags, a glassy amorphous phase obtained with faster cooling is generally preferred to crystallized mineral phases obtained with slower cooling. This is due to the effect of degree of crystallinity on the solidified slag

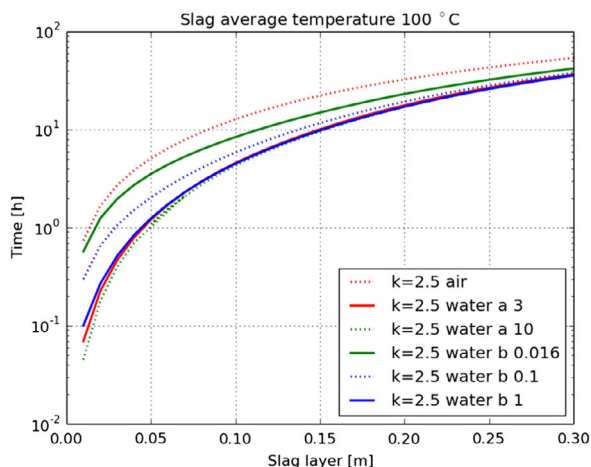


Figure 10. Calculated cooling time from 1600 to 100 °C under conditions of ambient air cooling or water cooling with five different water spray cooling rates (0.016, 0.1, 1, 3, and 10 kg m⁻² s⁻¹). The water spray model of Wendelstorf et al.^[31] is marked with “a,” and the model of Yao and Cox^[30] is marked with “b”.

properties, such as reactivity, leaching, and conductivities.^[21] Furthermore, problematic phases, such as dicalcium silicate, may form during the slower cooling of AOD slags and cause disintegration of larger particles into dust due to volumetric changes related to mineralogical changes as temperature decreases.^[34] If the crystallization during the cooling cannot be avoided, i.e., the cooling rate of the slag is not fast enough, the formation of the most harmful minerals, such as dicalcium silicate mentioned earlier, could be avoided by mixing different kinds of slags before the cooling and thus directing the slag composition into an area in which less harmful minerals are formed.^[35] Generally speaking, the amorphous structure is more easily obtained for slags with higher SiO₂ contents because the required cooling rates for the basic slags are extremely high.^[21]

4. Conclusions

A numerical model for slag layer cooling has been developed and tested. The results show that slag cooling is a relatively slow process due to the low thermal conductivity of slag. The use of water sprays for enhancing the cooling rate has a significant but limited effect: the inner part of the slag layer cools slowly, even with low surface temperatures. For rapid cooling, the slag layer should be very thin or broken into pieces.

Acknowledgements

This work was conducted within the Symbiosis of Metal Production and Nature (SYMMET) research program funded by Business Finland. V.-V.V. thanks the Walter Ahlström foundation for its funding.

Conflict of Interest

The authors declare no conflict of interest.

Keywords

heat transfer, numerical modeling, slag cooling

Received: January 31, 2020

Revised: May 28, 2020

Published online: June 25, 2020

- [1] International Stainless Steel Forum, Meltshop Production Statistics 2018, **2018**.
- [2] B. V. Patil, A. H. Chan, R. J. Choulet, *The Making, Shaping and Treating of Steel. 11th Edition Steel Making and Refining*, The AISE Steel Foundation, Pittsburgh, PA **1998**, pp. 715–741.
- [3] K. Pastucha, J. Spiess, S. Dimitrov, C. Bruckner, *AISTech2010*, Association for Iron & Steel Technology, Pittsburgh, PA **2010**.
- [4] W. Rubens, Doctoral Thesis, Clausthal University of Technology, Clausthal-Zellerfeld, Germany **1988**.
- [5] K. Koch, W. Münchberg, H. Zörcher, W. Rubens, *Stahl Eisen* **1992**, 112, 91.
- [6] W. Münchberg, K. Koch, H. Zörcher, W. Rubens, *Stahl Eisen* **1992**, 112, 49.
- [7] E. Schürmann, K. Rosenbach, *Arch. Eisenhüttenwes.* **1973**, 44, 761.
- [8] E.-P. Heikkinen, V.-V. Visuri, T. Fabritius, in *Proc. of the 8th European Oxygen Steelmaking Conf.*, Associazione Italiana di Metallurgia, Taranto **2018**.
- [9] G. Reiner, G. Mörtl, *Radex-Rundschr.* **1973**, 630.
- [10] W. Münchberg, *Stahl Eisen* **1980**, 100, 1051.
- [11] V.-V. Visuri, R. Mattila, P. Kupari, T. Fabritius, in *Proc. of the 7th Int. Congress on Science and Technology of Steelmaking*, Associazione Italiana di Metallurgia, Venice **2018**.
- [12] T. Haas, V.-V. Visuri, A. Kärnä, E. Isohookana, P. Sulasalmi, R. H. Eriç, H. Pfeifer, T. Fabritius, in *Advances in Molten Slags, Fluxes, and Salts: Proc. of the 10th Int. Conf. on Molten Slags, Fluxes and Salts 2016* (Eds: R. G. Reddy, P. Chaubal, P. C. Pistorius, U. Pal), The Minerals, Metals & Materials Society, Seattle, WA **2016**, pp. 999–1008.
- [13] P. Ternstedt, P. Ni, N. Lundqvist, A. Tillander, P. G. Jönsson, *Ironmak. Steelmak.* **2018**, 45, 944.
- [14] H.-J. Odenthal, U. Thiedemann, U. Falkenreck, J. Schlueter, *Metall. Mater. Trans. B* **2010**, 41, 396.
- [15] M. Lindvall, L. C. So, M. Mahdi, J. Bolen, J. Nell, I. Nolet, D. Metcalfe, S. Mostaghel, O. Sundqvist, *J. Sust. Metall.* **2019**, 5, 157.
- [16] Y. Pontikes, P. T. Jones, D. Geysen, B. Blanpain, *Arch. Metall. Mater.* **2010**, 55, 1167.
- [17] D. Durinck, S. Arnout, G. Mertens, E. Boydens, P. T. Jones, J. Elsen, B. Blanpain, P. Wollants, *J. Am. Ceram. Soc.* **2008**, 91, 548.
- [18] L. Kriskova, Y. Pontikes, L. Pandelaers, Ö. Cizer, P. T. Jones, K. Van Balen, B. Blanpain, *Metall. Mater. Trans. B* **2013**, 44, 1173.
- [19] M. Tossavainen, F. Engstrom, Q. Yang, N. Mena, M. L. Larsson, B. Bjorkman, *Waste Manage.* **2007**, 27, 1335.
- [20] M. Gautier, J. Poirier, F. Bodéan, G. Franceschini, E. Véron, *Int. J. Miner. Process.* **2013**, 123, 94.
- [21] C. A. Myers, T. T. Nakagaki, *ISIJ Int.* **2018**, 58, 211.
- [22] G. J. Ma, Y. Fang, T. Hui, *Adv. Mat. Res.* **2011**, 225–226, 812.
- [23] L. Pandelaers, A. D'Alfonso, P. T. Jones, B. Blanpain, *ISIJ Int.* **2013**, 53, 1106.
- [24] G. Liang, I. Mudawar, *Int. J. Heat Mass Transfer* **2017**, 115, 1174.
- [25] G. Liang, I. Mudawar, *Int. J. Heat Mass Transfer* **2017**, 115, 1206.
- [26] A. A. Tseng, M. Raudensky, T. W. Lee, *Heat Transfer Eng.* **2016**, 37, 1401.
- [27] J. Breitenbach, I. V. Roisman, C. Tropea, *Exp. Fluids* **2018**, 59, 55.
- [28] J. Ylipekkala, Master's Thesis, Luleå University of Technology, Luleå, Sweden **2005**.

- [29] Verein Deutscher Eisenhüttenleute, *Slag Atlas*, Verlag Stahleisen, Düsseldorf, Germany **1995**.
- [30] S. C. Yao, T. L. Cox, *Exp. Heat Transfer* **2002**, 15, 207.
- [31] J. Wendelstorf, K.-H. Spitzer, R. Wendelstorf, *Int. J. Heat Mass Transfer* **2008**, 51, 4902.
- [32] W. Edelbauer, D. Zhang, R. Kopun, B. Stauder, *Appl. Therm. Eng.* **2016**, 100, 1259.
- [33] A. Pola, M. Gelfi, G. M. La Vecchia, *J. Mater. Process. Technol.* **2013**, 213, 2247.
- [34] E.-P. Heikkinen, T. M. J. Fabritius, T. M. T. Kokkonen, J. J. Härkki, *Steel Res. Int.* **2004**, 75, 800.
- [35] E.-P. Heikkinen, V. Leinonen, P. Tanskanen, T. Fabritius, in *Proceedings of the 1st Int. Conference on Energy and Material Efficiency and CO₂ Reduction in the Steel Industry*, Iron and Steel Institute of Japan, Kobe **2017**.
- [36] D. R. Lide, *Handbook of Chemistry and Physics*, 84th ed., CRC Press, Boca Raton **2004**.
- [37] N. R. Pallas, Y. Harrison, *Colloid. Surf.* **1990**, 43, 169.
- [38] National Institute of Standards and Technology, *Thermophysical Properties of Fluid Systems, NIST Standard Reference Database Number 69*, National Institute of Standards and Technology, Gaithersburg, MD **2018**.